MAORY: optical configuration and expected optical performances

D. Magrin*[a], G. Pariani[b], M. Munari[c], A. Rakich[d], B. Delabre[e], J. Kosmalski[e], P. Rabou[f], A. Bianco[b], M. Bergomi[a], E. Radaelli[b], G. Rodeghiero[g,i], D. Greggio[a], L. Busoni[h], I. Foppiani[g], M. Riva[b], U. Di Giammatteo[g], P. Ciliegi[g].

[a]INAF – Osservatorio Astronomico di Padova, Vicolo dell'Osservatorio 5, 35122 Padova, Italy;
[b]INAF – Osservatorio Astronomico di Brera, Via Bianchi 46, 23807 Merate, Italy;
[c]INAF – Osservatorio Astrofisico di Catania, Via S. Sofia 78, 95123 Catania, Italy;
[d]Mersenne Optical Consulting, 41 Rimu Rd., Raumati Beach, Paraparaumu 5032 New Zealand;
[e]ESO, Karl-Schwarzschild-Strasse 2, D-85748 Garching bei München, Germany
[f]IPAG – Institut de Planétologie et d'Astrophysique de Grenoble, 414, Rue de la Piscine, Domaine Universitaire, 38400 St-Martin d'Hères, France;
[g]INAF – Osservatorio di Astrofisica e Scienza dello spazio, Via Piero Gobetti 93/3, 40129 Bologna, Italy;
[h]INAF – Osservatorio Astronomico di Arcetri, Largo Enrico Fermi 5, 50125 Firenze, Italy;
[i]INAF – Osservatorio Astronomico d'Abruzzo, Via M. Maggini snc, Teramo, Italy

ABSTRACT

The Multi Conjugate Adaptive Optics RelaY (MAORY) is the Multi-Conjugated Adaptive Optics (MCAO) module for the European Extremely Large Telescope (ELT). MAORY is one of the ELT first light instruments, designed to feed the Near Infrared Red (NIR) camera MICADO with both MCAO and Single-Conjugated AO (SCAO) operation modes. The optical configuration provides a one to one image of telescope focal surface on the MICADO focal surface (with the additional capability for a second port dedicated to a future instrument), and allows the implementation of two deformable mirrors together with the Laser Guide Star (LGS) and Natural Guide Star (NGS) channels for wavefront sensing and tomographic reconstruction. In this paper we present the status of the optical configuration in the Preliminary Design Review (PDR) framework for the main path optics and the analyses results on the expected optical performance.

Keywords: MAORY, ELT, Adaptive Optics, MCAO, MICADO

1. INTRODUCTION

The MAORY optical system [1][2] provides an almost one-to-one image of the ELT focal surface to the MICADO [3] entrance focal surface (science FoV) and to the 3 NGS Wavefront Sensor (WFS) focal surface (technical FoV) and to a second instrument port focal plane. The optical system splits images of infinitely distant sources from images of the 6 (up to 8) laser guide stars (LGS) generated at the sodium layer at a finite altitude by means of a dichroic filter. The LGS light is focused then on the entrance plane of the LGS WFS module by an objective. The optical system provides the possibility to accommodate up to two post focal deformable mirrors (DMs), conjugated at altitudes of 17.5 km and 6.5 km, and, together with the ELT M4, these provide the AO correction.

In the previous phases of the project, several optical solutions have been considered, spanning a range from parabolic mirrors designs to fully aspherical mirrors designs, from modified Offner designs to mixed aspherical/spherical designs [4][5][6]. The requirements also evolved through the conceptual design phases. In this proceeding, we describe the baseline for the PDR: MAORY Mirrors System (MMS) and the LGS Objective (LGSO).

*demetrio.magrin@inaf.it

Adaptive Optics Systems VII, edited by Laura Schreiber, Dirk Schmidt, Elise Vernet, Proc. of SPIE
Vol. 11448, 1144834 · © 2020 SPIE · CCC code: 0277-786X/20/$21 · doi: 10.1117/12.2562427

2. BASELINE DESIGN

2.1 MAORY Mirrors System

The MMS configuration has been initially proposed by Bernard Delabre. It is based on 4 powered mirrors (2 aspherical and 2 spherical) able to deliver high quality in terms of WFE and field distortion. It is highly tolerant to defocus and astigmatism aberrations that can be compensated by acting on the last mirror with power. This configuration implements also the concept first introduced by Andrew Rakich of using an aspherical plate near the telescope focal surface to allow for the correction of multiple object conjugate distances [7][8][9]. By adding this correcting plate close to the entrance focal surface it is possible to greatly improve the quality of the exit pupil image, of the DMs meta-pupil image and of the LGS images at different conjugation altitudes, without degrading the quality for the infinite conjugated surface. We have re-optimized and adapted the general optical solution to the MAORY specific requirements and constraints. A scheme of the MMS is shown in Figure 1.

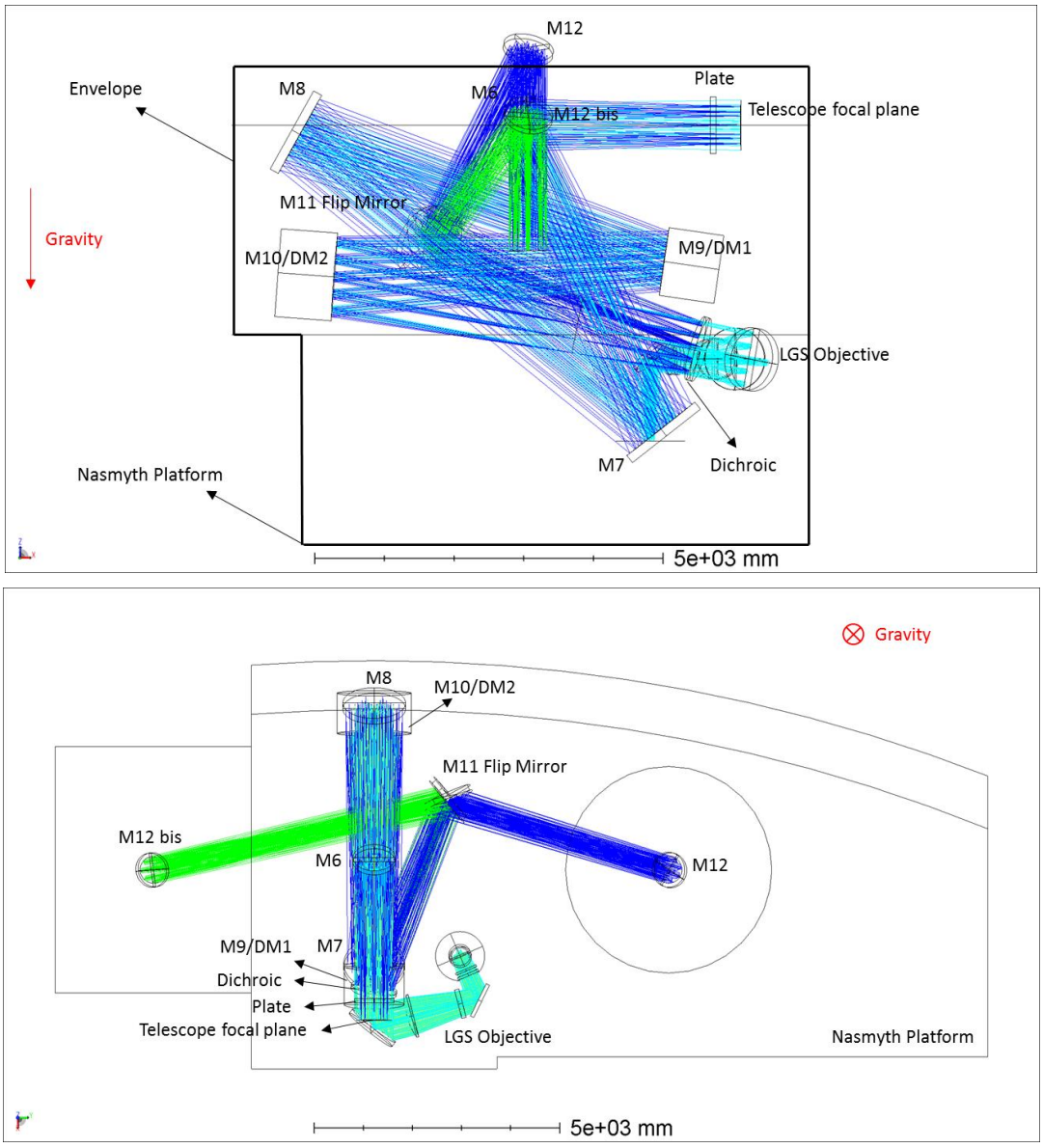

Figure 1. MMS side view layout (top) and top view layout (bottom). Blue rays represent the science and NGS path to MICADO, green rays represent the science and NGS path to second instrument, Cyan rays represent the LGS path.

The F/17.75 beam incoming from the ELT focal surface initially passes through the correcting plate. It is a window that thermally separates the external and internal environment. The second surface of the correcting plate is aspherical and allows increasing the quality of multiple object conjugated distances. Following the path, there is a first flat mirror, M6, folding the beam down to the first aspherical concave mirror M7. The beam is reflected up to the second aspherical concave mirror M8, and then down again towards the first DM, M9, having spherical surface. This mirror is the only convex surface of the main path. After that the beam is reflected by the second DM, M10, which is concave and spherical. All the other optical surfaces downstream M10 are flat.

After M10, the image of the pupil is formed, and just after this image the light is separated between science and NGS light and LGS light by means of a dichroic filter. The LGS light (589 nm) is transmitted, while science and NGS light (>600nm-2400nm) is reflected. The reflected light then reaches M11, a flat flip mirror that allows the selection of the MICADO path or of the second instrument path through a rotational axis. Finally, the light is reflected by a flat mirror, M12 (or M12 bis), installed over MICADO (or, as previously mentioned, some future second instrument) and comes to a focus at the gravity invariant entrance focal surface of the instruments. MICADO and the second instrument share the DMs and the LGS WFS module, while the NGS WFS module is duplicated. focal surfaces delivered to MICADO and to the second instrument have the same nominal performance characteristic.

Most of optical elements extend along a plane perpendicular to the ELT focal surface and to the Nasmyth platform. Such a solution has been adopted in order to lower the center of gravity of the whole system (the ELT focal surface is located at 6 m above the Nasmyth platform) and to reduce the overall pace-envelope. The mass budget is indeed quite limited forcing the opto-mechanical bench to develop along the vertical direction, increasing the stability but also the AIV and maintenance process complexity.

2.2 LGS Objective

The LGS Objective (LGSO) reduces the LGS beam F/# at wavelength 589 nm from about 19 at the dichroic to 5 at the LGS WFS module entrance focal surface. It is composed by 4 silica spherical lenses and three fold mirrors (see Figure 2). The first two mirrors have been introduced in order to maintain the objective within the available envelope, while the third mirror allows to feed the LGS module with a gravity invariant and telecentric focus. The LGS asterism required by MAORY is fixed to field angle 45 arcsec with a FoV of ± 16.8 arcsec (LGS elongation). As the ELT declination angle varies (Zenith angle 0-60 degrees), the LGS launchers will maintain the LGS sources on the sodium layer at the fixed angle of 45 arcsec. Thanks to the telecentric beam delivered by the LGSO, the radial coordinate of the LGS images on the LGSO focal surface will not change as the apparent altitude (84-180 km) of the sodium layer varies. In this way, the LGS module just needs to rotate around its central axis and to move up and down in order to follow the declination variation effect.

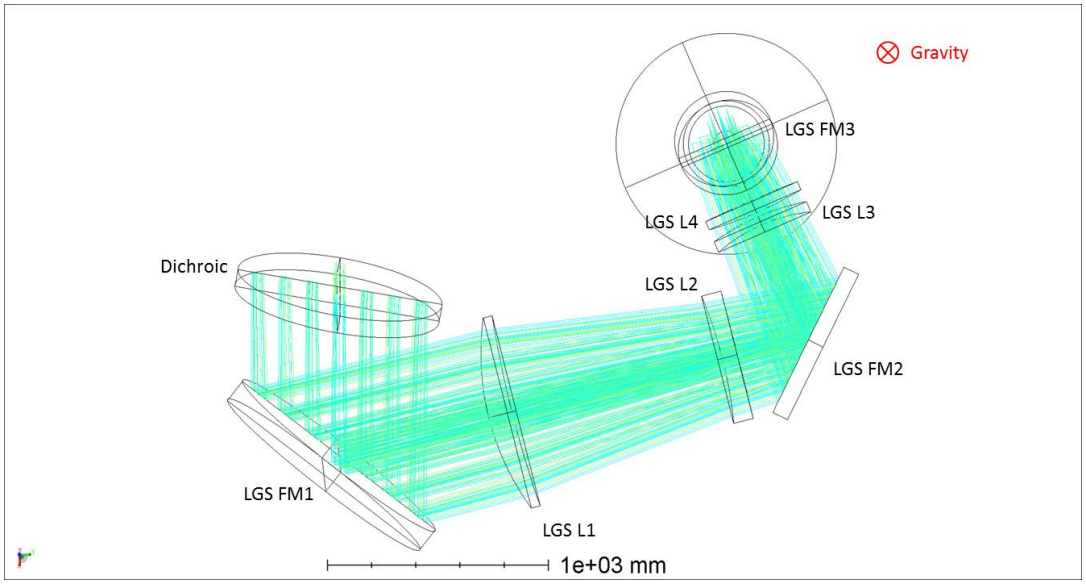

Figure 2. LGSO top view layout. The two colors represent rays incoming from two different LGS apparent conjugation altitudes.

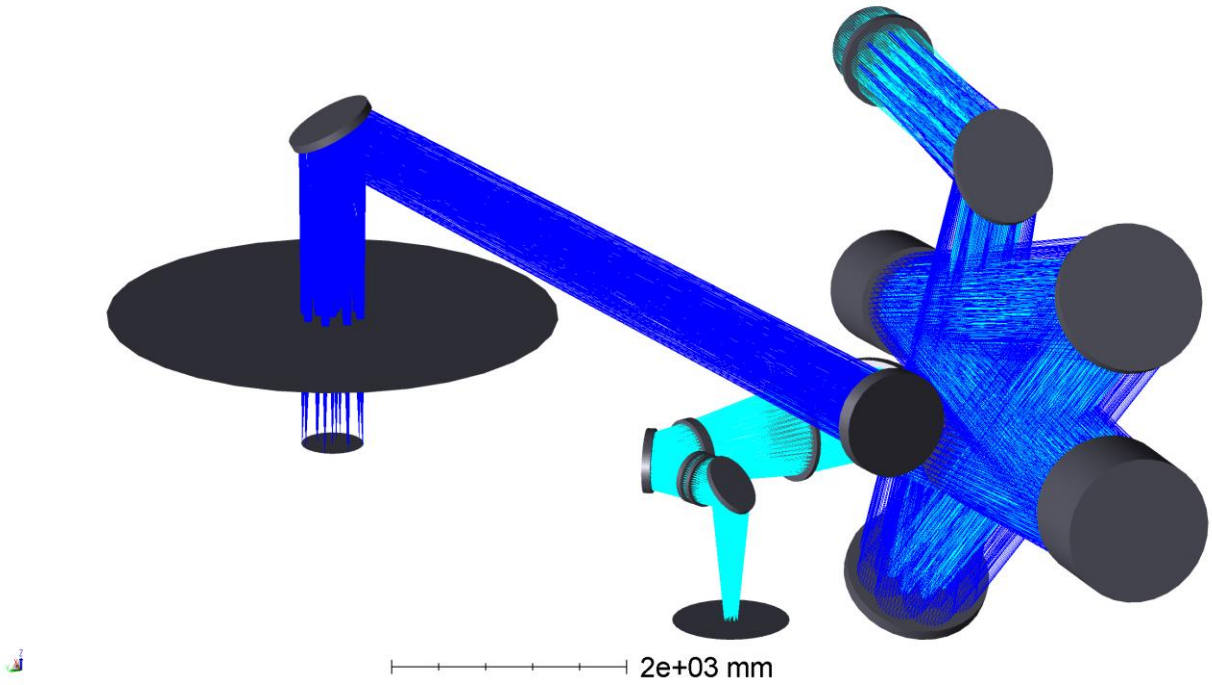

Figure 3. 3D view of the MAORY optical configuration. Blue rays represent the science and NGS path to MICADO, Cyan rays represent the LGS path.

2.3 Optical system parameters and optics prescription data

The main optical parameters of the main path and the LGS path are reported in Table 1.

MAIN PATH		
Image space F/#	17,755	
Effective focal length	684302	mm
Plate scale	0,3014	arcsec/mm
Entrance dupil Diameter	38542	mm
Entrance pupil obstruction diameter	10952	mm
Scientific FoV diameter	76	arcsec
Technical FoV diameter	160	arcsec
Field curvature	infinity	mm
Exit pupil distance	14361	mm

LGS PATH		
Image space F/#	5,025	
Sodium layer conjugation range	84-180	km
Effective focal length	193645	mm
Plate scale	1,065	arcsec/mm
LGS asterism radius	45	arcsec
LGS FoV	±15	arcsec
Field curvature	infinity for 45 arcsec asterism	mm
Exit pupil distance	infinity	mm

Table 1. Main optical parameters of the main path (left) and the LGS path (right).

The optics prescription data in the local coordinates system are reported in Table 2 and Table 3 for the MMS and LGSO respectively.

3. MMS NOMINAL PERFORMANCE

Given that MICADO is mainly a NIR imager with science cases driven also by astrometry, we present here the optical performance delivered by MAORY to the MICADO entrance focal surface in terms of RMS wavefront error (WFE), intra-epoch distortion variation and inter-epoch distortion variation. The WFE in terms of the RMS WFE maps at wavelength 1 µm, 1.65 µm and 2.2 µm in the technical and in the MICADO FoV are shown in Figure 4. The entrance correcting plate introduces a pure chromatic focal shift at the delivered focal surface. Assuming the focal surface position at 1 µm as reference, the best focal surfaces at 1.65 µm and 2.2 µm are located at 0.309 mm and 0.629 mm, respectively.

MMS main path

	type	Surface	Radius of curvature [mm]	Thickness optic/substrate [mm]	Material	Concavity
Plate	entrance window	S1	infinity	85	suprasil 3002	Flat
		S2	infinity			Flat
M6	Fold 1		infinity	100	zerodur	Flat
M7	Free Form 1		-35094,937	124	zerodur	CV
M8	Free Form 2		38403,193	128	zerodur	CV
M9 DM1 Simulacrum	Deformable Mirror		15456,015	98	zerodur	CX
M10 DM2 Simulacrum	Deformable Mirror		14946,890	126	zerodur	CV
Dichroic	Dichroic	S1	infinity	80	suprasil 3002	Flat
		S2	infinity			Flat
M11	Fold2-Flip mirror		infinity	122	zerodur	Flat
M12	Fold 3		infinity	78	zerodur	Flat

	Aspheric terms						
	type [mm]	Normalization radius [mm]	Z6 [mm]	Z7 [mm]	Z9 [mm]	Z11 [mm]	Z12 [mm]
Plate							
	Zernike Standard Sag	350	8,02336E-02	9,06846E-03	-2,52709E-04	-1,14298E-03	
M6							
M7	Zernike Standard Sag	570,240	1,33808E-02	9,15126E-03	3,88534E-04	8,19550E-04	3,21440E-05
M8	Zernike Standard Sag	585,621	6,04576E-02	6,01545E-03	1,76372E-04	3,59100E-04	3,84119E-06
M9 DM1 Simulacrum							
M10 DM2 Simulacrum							
Dichroic							
M11							
M12							

	Aperture type	Clear Aperture [mm]	Mechanical Aperture [mm]	Aperture decenter X[mm]; Y[mm]	Coating
Plate	circular	710	810	0; 0	AR (0.589-2.4 µm)
	circular				
M6	elliptical	760x900	860x1000	0; 10	Protected Silver
M7	circular	1140	1240	0; 0	Protected Silver
M8	circular	1180	1280	0; 0	Protected Silver
M9 DM1 Simulacrum	circular	880	980	0; 0	Protected Silver
M10 DM2 Simulacrum	circular	1164	1264	0; 0	Protected Silver
Dichroic	circular	840	940	0; 0	Special
	circular			0; 0	AR (0.589 µm)
M11	elliptical	1120x820	1220x920	7; 3	Protected Silver
M12	elliptical	600x674	700x774	0; -2	Protected Silver

Table 2. Optics prescription data for the MMS.

MMS LGS Objective

	type	Surface	Radius of curvature [mm]	Thickness [mm]	Material
LGS FM1	Fold 1		infinity	111	zerodur
LGS L1	meniscus	S1	-1210,000	108	silica
		S2	-5621,000		
LGS L2	plano-concave	S1	2077,000	70	silica
		S2	infinity		
LGS FM2	Fold 2		Infinity	74	zerodur
LGS L3	meniscus	S1	-746,700	40	silica
		S2	-1031,500		
LGS L4	biconvex	S1	1831,500	60	silica
		S2	-4943,000		
LGS FM3	Fold 3		Infinity	60	zerodur

	Concavity	Aperture type	Clear Aperture [mm]	Mechanical Aperture [mm]	Aperture decenter X[mm]; Y[mm]	Coating
LGS FM1	Flat	elliptical	1010x800	1110x900	1; 0	Protected Silver
LGS L1	CX	circular	788	888	0; 0	AR (0.589 µm)
	CV					AR (0.589 µm)
LGS L2	CV	circular	534	594	0; 0	AR (0.589 µm)
	CX					AR (0.589 µm)
LGS FM2	Flat	elliptical	632x484	732x584	-18; 0	Protected Silver
LGS L3	CV	circular	416	456	0; 0	AR (0.589 µm)
	CX					AR (0.589 µm)
LGS L4	CX	circular	414	454	0; 0	AR (0.589 µm)
	CX					AR (0.589 µm)
LGS FM3	Flat	elliptical	354x500	454x600	0; -25	Protected Silver

Table 3. Optics prescription data for the LGSO.

These shifts can be compensated during the pre-set by offsetting the NGS WFS position or the defocus signal in the AO loop, depending on the filter band of the observation. After the chromatic focal shift, the maximum nominal WFE delivered by MMS main path in the MICADO FoV is about 20 nm, while in the technical FoV is about 75 nm as shown in the figure.

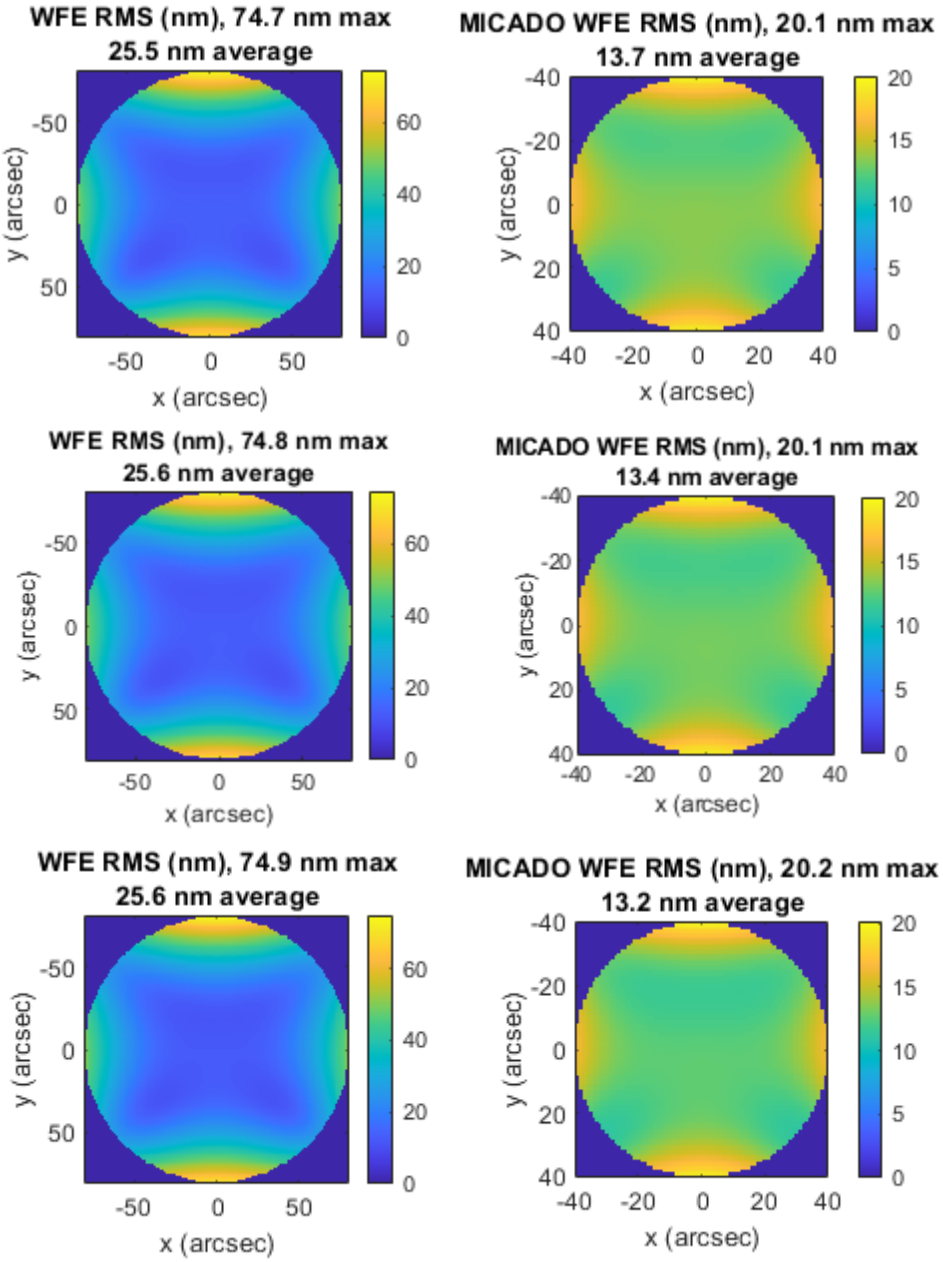

Figure 4. RMS wavefront map over the technical FoV (left) and MICADO FoV (right) at wavelength 1 µm (top), 1.65 µm (middle) and 2.2 µm (bottom). Color bar units are nanometers.

During an observation, MICADO rotates around its entrance optical axis in order to compensate the rotation introduce by the ELT tracking science targets. In principle, during the observation, the sources footprints on the MICADO optics and their images in the detector are fixed. This means also that any field distortion introduced by MICADO can be calibrated and is static. Conversely, in MAORY, as the ELT image delivered from ELT to MAORY rotates, the source optical footprints move across the optics and, as consequence, any variation in the field distortion of MAORY is seen by

MICADO. The variation of the field distortion within a single exposure is called intra-epoch distortion variation, while between different exposures is called inter-epoch distortion variation.

The intra-epoch distortion variation not only impacts on the source centroid shift, causing blurring, but also on the reference stars positions obtained by the NGS WFS and used for low order sensing. The NGS WFS module indeed is co-rotating with MICADO. If one of the reference stars experiences a centroid shift due to MAORY field distortion variation, the signal is propagated by the WFS through the AO loop and the effect is to introduce a distortion variation also on the MICADO FoV.

The worst case we have assumed is an astrometric observation of 120 sec with target altitude equal to 80 degrees. At the ELT latitude, it translates on a maximum rotation of the field of 2.6 degrees. We have simulated the intra-epoch distortion variation by considering a regular grid of fields, having a spacing of 1 arcsec, over the technical FoV. We have then rotated the ELT elevation angle by 2.6 degrees and counter-rotated MICADO by the same angle, as shown in Figure 5. By comparing the centroids coordinates before and after the rotation/counter-rotation, we have computed the distortion variation map in the case of intra-epoch. The results are shown in Figure 6. The maximum distortion variation is at wavelength 2.2 μm with a modulus variation of the centroid position of about 1.5 micron, corresponding to 0.5 mas.

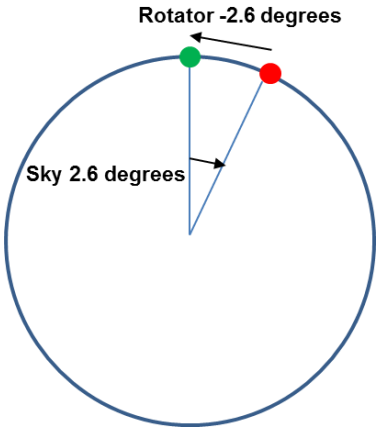

Figure 5. Scheme of the intra-epoch distortion variation with ELT elevation angle rotation and MICADO counter rotation.

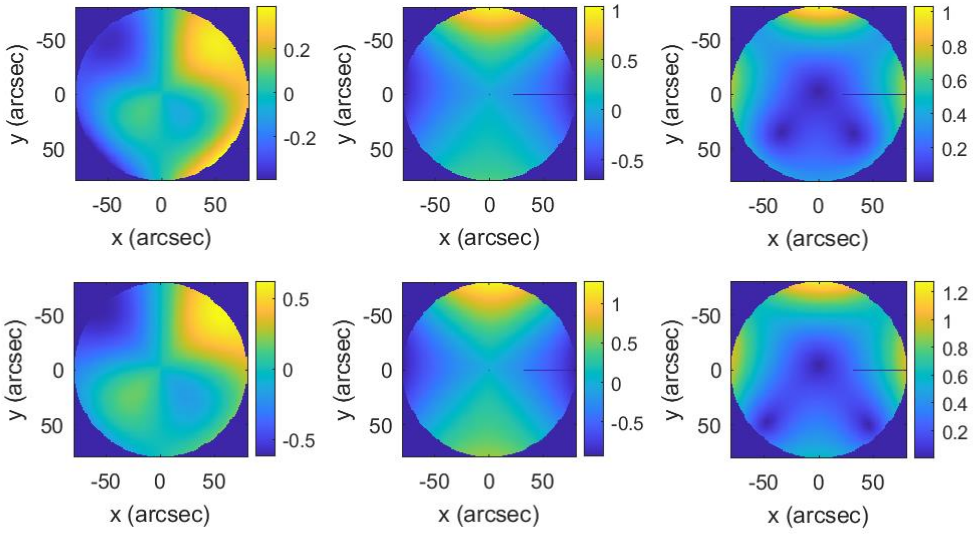

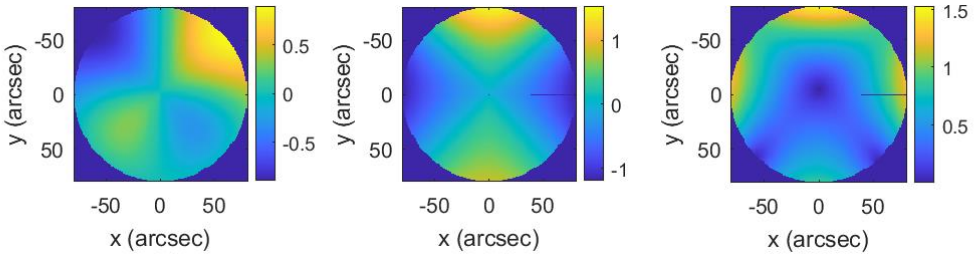

Figure 6. Radial component (first column), tangential component (second column) and modulus (third column) of the intra-epoch distortion variation computed at wavelength 1 µm (top), 1.65 µm (middle) and 2.2 µm (bottom) over the technical FoV. Color bar units are micron.

The inter-epoch distortion variation refers to the capability to perform relative astrometric measurement between a pair of stars 1 arcsec apart observed at different epochs. Such technique assumes, as part of the reduction process, the application of an astrometric polynomial fit correction between the two images [10]. In order to simulate the inter-epoch distortion variation, we have considered the centroid positions corresponding to a set of test stars placed over a regular square grid, with spacing of 1 arcsec, over the MICADO FoV. We have computed the centroid positions of the grid over the full range of MICADO rotation angles (up to 180 degrees given the optical system symmetry) with steps of 5 degrees. We have assigned the grid at 0 degrees to be the reference image and this is compared to subsequent images. The analysis has been limited to two sources having 1 arcsec relative distance. We have computed the residuals of the astrometric polynomial fit correction up to 3rd. The results are shown in Figure 7. In the figure, the central mark of the boxplot indicates the median, and the bottom and top edges of the box indicate the 25th and 75th percentiles, respectively. The whiskers extend to the most extreme data points. Already after the 1st order polynomial fit correction (plate scale), for the nominal design, the residuals are below 90 µas over the whole range of MICADO rotation angles. After the 3rd order polynomial fit correction (geometric distortion), the residuals are always below 6 µas.

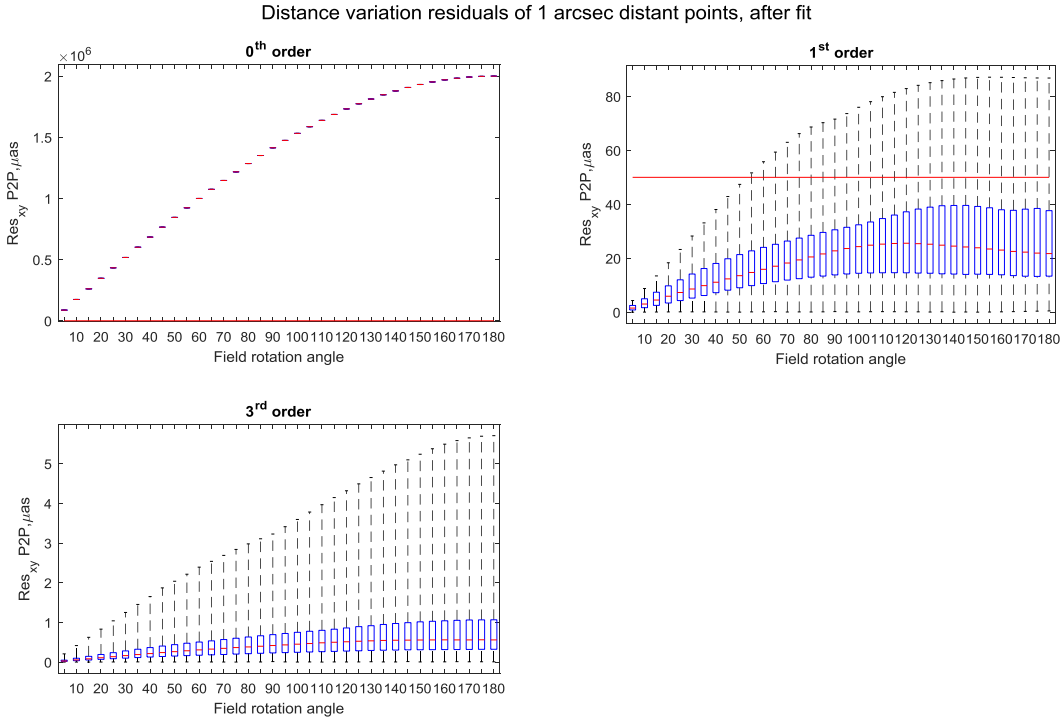

Figure 7. Residuals between two stars having on sky distance 1 arcsec as function of the MICADO rotation angle o, assuming the reference distortion map at 0 degrees, after applying no correction, a 1st order polynomial fit correction, a 3rd order polynomial fit correction. Units are µas. The MICADO distortions are not taken into account. The red horizontal line represents the MICADO astrometric requirement.

4. MMS TOLERANCE SIMULATION AND EXPECTED PERFORMANCE

The tolerance simulation accounts for manufacturing errors and alignment compensations and residuals. We require a characterization of each opto-mechanical subsystems with specific precision and accuracy. In particular, we assume to know the position of the optical surfaces with respect to mechanical fiducials (SMRs) and have also "as manufactured values" for the radius of curvature/defocus and astigmatism surface error. For higher order surface error, we require a certain accuracy. The alignment procedure is based on the positioning the opto-mechanics using a laser tracker. After this initial positioning, MMS is aligned using as degrees of freedom the piston and tip/tilt movements of M10 to re-optimize the WFE by minimizing defocus and astigmatisms over 5 fields in the MICADO FoV and the tip/tilt of M11 and M12 to re-align the focal surface and the exit pupil to MICADO.

The tolerance procedure for the main path has been implemented in three steps:

1. As-built alignment: we assume to reposition opto-mechanical subsystems after the as-built measurements are provided by the manufacturers. Only low-order manufacturing errors are considered and with infinite precision.
2. High order manufacturing errors: we introduce the high-order manufacturing errors and this introduces was not used in step 1.
3. Characterization errors and alignment: we introduce the uncertainties on the low-orders manufacturing errors used in step 1, the characterization errors of the surface knowledge and we apply the alignment procedure.

The tolerance process has been simulated by means of Monte Carlo (MC) approach. The simulations and the analysis have been implanted on Amazon HTC cloud platform [11][12]. The parameter driving the process was the WFE.

In step 1, we have simulated 3000 MC occurrences assuming a parabolic statistic for the errors distribution. The parabolic statistic is pessimistic; however, it is mimicking somehow the fact that, for some manufacturing parameters, the providers will limit the manufacturing time to the minimum, i.e. just after the match of the specification. We have selected a 98-percentile occurrence in terms of WFE as input for the next step. This choice allows excluding outliers, due to limited optimization cycles, and counterbalancing the pessimistic statistic. As in step 1, in the step 2 we have simulated 3000 MC occurrences assuming a parabolic statistic for the errors distribution, starting from the selected 98-percentile occurrence. We have then selected a 98-percentile occurrence in terms of WFE from the step 2 distribution as input for the next step. Using as starting point the 98-percentile occurrence of step 2, in the step 3 we have simulated 3000 MC occurrences assuming a uniform statistic for the errors distribution. This choice is pessimistic given that the measurement uncertainties have typically a normal distribution. We have then selected a 98-percentile occurrence in terms of WFE. This last occurrence represents the WFE we expect to have after the manufacturing and characterization of the opto-mechanics and the alignment process. Even if the distortion variation is not correlated with the WFE, in all the three steps we have selected the 98-percentile occurrence also in terms of distortion variation.

The WFE in terms of the RMS WFE maps has been computed for each occurrence. In Figure 8, the MC distribution after the step 3 is shown. The 98 percentile of the RMS WFE in the MICADO FoV has an average value of about 74 nm and a maximum value of about 96 nm. The 98 percentile of the RMS WFE in the Technical FoV has an average value of about 97 nm and a maximum value of about 153 nm. The WFE budget of MMS is 150 nm in the MICADO FoV.

The intra-epoch distortion variation has been computed for each occurrence. In Figure 9, the MC distribution after the step 3 is shown. The 98 percentile of the intra-epoch distortion variation in the MICADO FoV has an average value of about 1.9 μm (0.6 mas) and a maximum value of about 3.4 μm (1.0 mas). The 98 percentile of the intra-epoch distortion variation in the technical FoV has an average value of about 3.7 μm (1.1 mas) and a maximum value of about 6.9 μm (2.1 mas). The intra-epoch distortion variation error budget of MMS is 12.6 μm (3.8 mas).

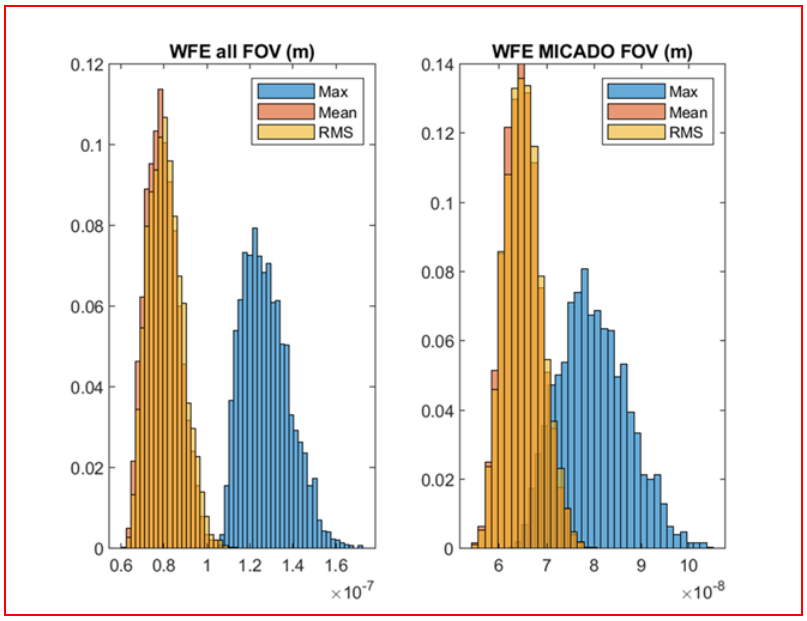

Figure 8. Average value, RMS value and maximum value of the RMS WFE maps in the technical and the MICADO FoV after the tolerance process. Units are meters.

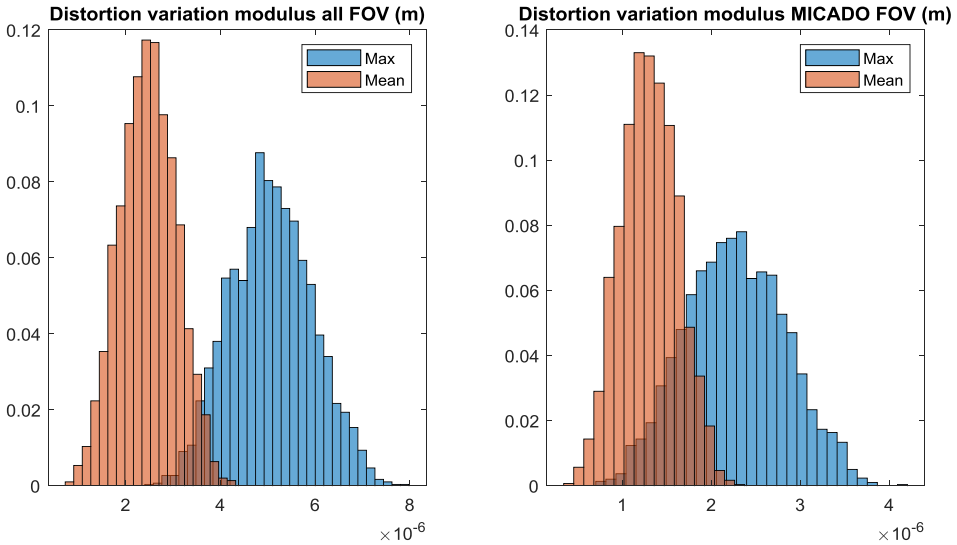

Figure 9. Average and maximum modulus value of the intra-epoch distortion variation in the technical and the MICADO FoV after the tolerance process. Units are meters.

The inter-epoch field distortion variation is a quite computing time consuming analysis to be applied statistically. We have assumed that there is correlation between the intra-epoch and the inter-epoch distortion variation. The analysis has been done on a 98-percentile occurrence of the intra-epoch distortion variation distribution. Results are shown in Figure 10. Already after the 1st and the 3rd order polynomial fit correction, the residuals are below 50 µas on a MICADO rotation angle within ± 25 degrees. By applying also the 5th order polynomial fit correction, the residuals are always below 50 µas.

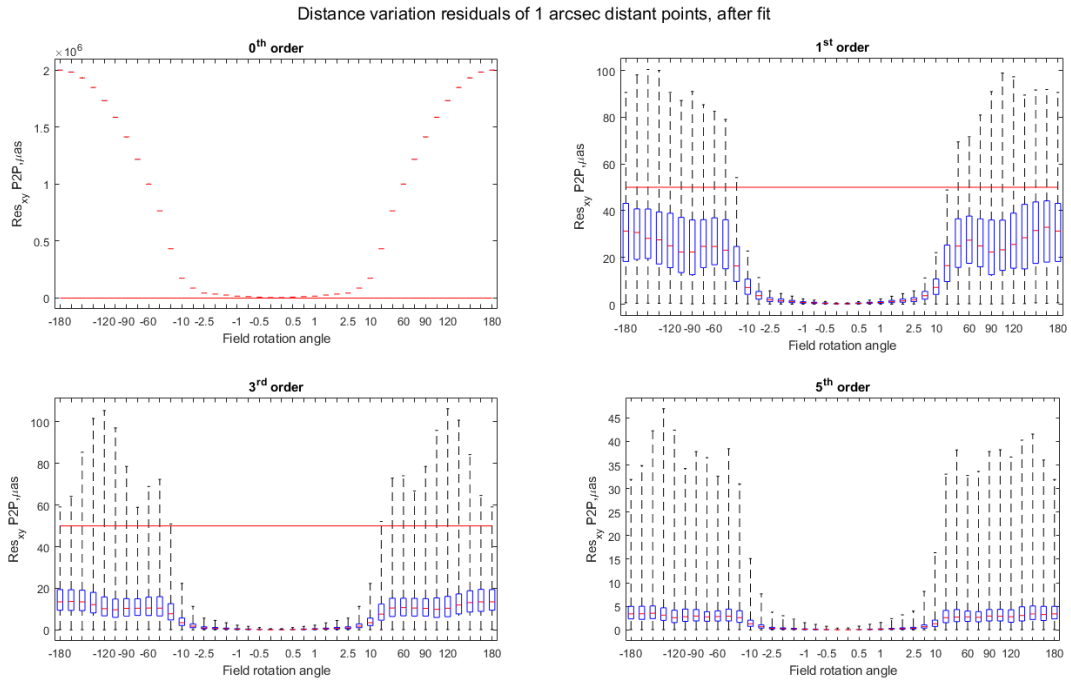

Figure 10. Residuals between two stars having on sky distance 1 arcsec as function of the MICADO rotation angle o, assuming the reference distortion map at 0 degrees, after applying no correction, a 1st order polynomial fit correction, a 3rd order polynomial fit correction and 5th order polynomial fit correction. Units are μas. The red horizontal line represents the MICADO astrometric requirement.

REFERENCES

[1] P. Ciliegi, et al. "MAORY: the adaptive optics module for the Extremely Large Telescope (ELT)", Proc. SPIE, this conference.

[2] P. Ciliegi, et al. "MAORY: a multi-conjugate adaptive optics relay for E-ELT", ESO Messenger, No.182, December 2020, in publication.

[3] R. Davies, J. Alves, Y. Clenet, et al., "The MICADO first light imager for the ELT: overview, operation, simulation", Proc. SPIE 10702, Ground-based and Airborne Instrumentation for Astronomy VII, 107021S (30 July 2018); https://doi.org/10.1117/12.2311483

[4] I. Foppiani, E. Diolaiti, M. Lombini, et al., "MCAO for the E-ELT: preliminary design overview of the MAORY module", 1st AO4ELT conference - Adaptative Optics for Extremely Large Telescopes, held 22-26 June, 2009 in Paris, France. Edited by Y. Clénet, J.-M. Conan, Th. Fusco, and G. Rousset. EDP Sciences, 2010, id.02013; DOI 10.1051/ao4elt/201002013

[5] E. Diolaiti, P. Ciliegi, R. Abicca, et al. "MAORY: adaptive optics module for the E-ELT", Proceedings of the SPIE, Volume 9909, (2016), July 2016, DOI: 10.1117/12.2234585

[6] M. Lombini, E. Diolaiti, M. Patti, "Historic evolution of the optical design of the Multi Conjugate Adaptive Optics RelaY for the Extremely Large Telescope", Monthly Notices of the Royal Astronomical Society, Volume 486, Issue 1, p.320-330, June 2019, DOI 10.1093/mnras/stz810

[7] A. Rakich, J.R. Rogers, "A Maxwellian "Ideal Imager" optical relay suitable for AO applications", Proc. SPIE, this conference.

[8] A. Rakich, J.R. Rogers, "Aberration theory-based approaches to optical design", Proc. SPIE, Proceedings Volume 11548, Optical Design and Testing X; 115480M (2020), https://doi.org/10.1117/12.2573666

[9] Rakich, A. "Optical systems capable of forming highly corrected images of 3-dimensional objects", International Patent Application No. PCT/NZ2020/050105 (publication pending)

[10] G. Rodeghiero, C. Arcidiacono, J.-U. Pott, et al., “Performance and limitations of using ELT and MCAO for 50 μas astrometry”, Proc of SPIE, 2020, this conference.
[11] Landoni, Marco; Taffoni, Giuliano; Bignamini, Andrea; Smareglia, Riccardo, “Application of Google Cloud Platform in Astrophysics”, Astronomical Data Analysis Software and Systems XXVIII. ASP Conference Series, Vol. 523, proceedings of a conference held (11-15 October 2018) at The Hotel at the University of Maryland, College Park, Maryland, USA. Edited by Peter J. Teuben, Marc W. Pound, Brian A. Thomas, and Elizabeth M.Warner. San Francisco: Astronomical Society of the Pacific, 2019, p.373.
[12] Landoni, M.; Romano, P.; Vercellone, S.; Knödlseder, J.; Bianco, A.; Tavecchio, F.; Corina, A.. “A Cloud-based Architecture for the Cherenkov Telescope Array Observation Simulations: Optimization, Design, and Results”, The Astrophysical Journal Supplement Series, Volume 240, Issue 2, article id. 32, 7 pp. (2019).